

## Velocity Map Imaging Study of Charge-Transfer and Proton-Transfer Reactions of CH<sub>3</sub> Radicals with H<sub>3</sub><sup>+</sup>

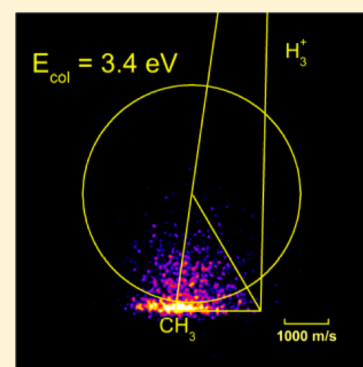
Linsen Pei,<sup>†</sup> Eduardo Carrascosa,<sup>‡</sup> Nan Yang,<sup>†</sup> Stefano Falcinelli,<sup>§</sup> and James M. Farrar<sup>\*,†</sup>

<sup>†</sup>Department of Chemistry, University of Rochester, Rochester, New York 14627, United States

<sup>‡</sup>Institut für Ionenphysik und Angewandte Physik, Universität Innsbruck, Technikerstraße 25/3, 6020 Innsbruck, Austria

<sup>§</sup>Dipartimento di Ingegneria Civile ed Ambientale, Università degli Studi di Perugia, 06125 Perugia, Italy

**ABSTRACT:** The velocity map imaging method has been applied to crossed beam studies of charge transfer and proton transfer between methyl (CH<sub>3</sub>) radicals formed by pyrolysis and H<sub>3</sub><sup>+</sup> cations over the collision energy range from 1.2 to 3.4 eV. Vibrational excitation in the H<sub>3</sub><sup>+</sup> reactants plays an important role both in promoting endoergic charge transfer and in supplying energy to the products of the proton-transfer reaction. Excited H<sub>3</sub><sup>+</sup> reactants with vibrational energy in excess of the barrier lead to energy-resonant charge transfer via long-range collisions. A small fraction of collisions that take place at low impact parameters appear to form charge-transfer products with higher levels of internal excitation. The proton-transfer reaction exhibits direct, stripping-like dynamics. Consistent with the kinematics of proton transfer, incremental kinetic energy supplied to the reactants is strongly directed into product relative kinetic energy, as predicted by the concept of “induced repulsive energy release”.



The study of chemical reactions of atomic and molecular ions with stable molecules is a subject as old as mass spectrometry itself,<sup>1</sup> and it is well-recognized that ion–molecule reactions are among the fastest known gas-phase processes.<sup>2</sup> In contrast, reactions of ions with polyatomic free radicals, especially hydrocarbon-based species, are much less well-studied. The presence of significant concentrations of ionic and free radical species in chemically energetic environments such as combustion, planetary atmospheres, and interstellar space suggests that ion–radical reactions should be important in determining the composition and energy content of such complex systems. Nevertheless, experimental examples of such reactions are few in number. Bierbaum and Ellison and co-workers<sup>3,4</sup> have reported the first study that probes the rates for reactions of ions with polyatomic hydrocarbon-based free radicals. In that work, proton-transfer rate constants from H<sub>3</sub>O<sup>+</sup> to allyl radicals and *o*-benzyne diradicals prepared by pyrolysis were measured in a selected ion flow tube. Rate constants were reported with large error limits because of difficulties in measuring reactant concentrations. Russell et al.<sup>5</sup> reported a Fourier transform ion cyclotron resonance study of the reactions of the benzyl cation with allyl radicals produced by flash pyrolysis, providing evidence for the formation of new C–C bonds. Most recently, the Viggiano lab<sup>6</sup> reported on the reactions of Ar<sup>+</sup> and O<sub>2</sub><sup>+</sup> with CH<sub>3</sub> radicals produced by dissociative electron attachment to CH<sub>3</sub>I and monitored by variable electron and neutral density attachment mass spectrometry (VENDAMS). The study yielded accurate rate constants and demonstrated that charge transfer to form CH<sub>3</sub><sup>+</sup> and fragments was the dominant process for both ions.

The development of a reliable, intense source of free radicals by Chen and co-workers<sup>7,8</sup> based on supersonic expansion of

gas containing an appropriate radical precursor and subsequent pyrolysis in a heated SiC tube following the nozzle has made these initial studies possible. However, experiments that probe the mechanistic and dynamical details of reactive collisions, especially energy disposal and product angular distributions, have not yet been reported, primarily because of low concentrations of reactive species.

Crossed molecular beam experiments that measure product velocity distributions afford an effective technique for elucidating reaction dynamics on ion–molecule systems, but traditional experiments employing an electrostatic energy analyzer detector swept over a range of lab energies and rotated through a range of laboratory scattering angles suffer from the shortcoming that in any detection time interval, the flux from only a single product velocity space element can be measured. In contrast, velocity space imaging methods, first introduced by Chandler and Houston<sup>9</sup> and subsequently refined by a number of investigators, most notably Eppink and Parker,<sup>10</sup> have been shown to allow detection of all possible velocity space elements in a single time window. The velocity map imaging (VMI) method, in which reaction products with specific velocity components parallel to the plane of the crossed beams focus to a single spot in the detection plane independent of their position in the collision volume, has been applied to a large number of photodissociation and bimolecular collision systems.<sup>11</sup> Despite the short duty cycle for such an experiment, the multiplex advantage of velocity mapping significantly increases the rate of data collection and makes experiments

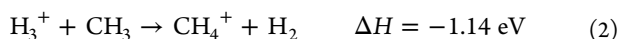
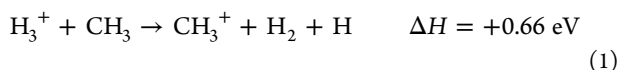
**Received:** March 11, 2015

**Accepted:** April 17, 2015

with reactive species produced in low concentrations possible. Wester and co-workers<sup>12–15</sup> and, more recently, the present group<sup>16,17</sup> have used the VMI method with delayed pulse extraction to determine product energy disposal for ion–molecule reactions studied in crossed beams.

In this Letter, we report the first crossed beam study of reactions of ions with polyatomic free radical reagents, exploiting the VMI method to determine velocity space distributions of reaction products and corresponding kinetic energy and angular distributions. We report results for charge transfer and proton transfer between  $\text{H}_3^+$  reactants and  $\text{CH}_3$  radicals produced in a pyrolysis source consisting of a SiC “afterburner” connected to a solenoid valve-based supersonic nozzle.

The specific reactions studied here are as follows



The enthalpy of formation of  $\text{H}_3^+$  was determined from the tabulated proton affinity of  $\text{H}_2$ ; all other standard enthalpies of formation are taken from the literature.<sup>18</sup>

Both reactants in this study have been highlighted as important reactive species in planetary upper atmospheres and in the interstellar medium. Oka and collaborators<sup>19</sup> have focused special attention on  $\text{H}_3^+$  as the most abundantly produced interstellar molecular ion, and its detection in the optical spectra of the outer atmospheres of Jupiter and Uranus<sup>20,21</sup> and in molecular clouds<sup>22</sup> underscores its importance in astrochemistry. Likewise, the methyl radical was first detected in our galaxy 15 years ago by the European Space Agency’s ISO infrared space telescope and has been labeled as one of the most important tracers for complex carbon-based molecules.<sup>23</sup>

In the experiments described here, a beam of  $\text{H}_3^+$  is formed by ion–molecule reactions in an electron impact ion source operating with a high pressure of  $\text{H}_2$ . It is well-known that this method results in vibrationally excited  $\text{H}_3^+$ , the extent of internal excitation depending on the number of collisions experienced in the ion source.<sup>24,25</sup> On the basis of calculations reported by Smith and Futrell,<sup>25</sup> as well as recent imaging studies from our group<sup>26</sup> on the  $\text{D}_3^+ + \text{CH}_4$  reaction, the reactant ion beam contains significant populations of vibrationally excited ions with internal energies above 1 eV.

The ion beam intersects a  $\text{CH}_3$  beam between two parallel electrode plates that define an equipotential volume. Mass-selective detection of both products is achieved by varying the delay times between extraction from the collision volume and gating the imaging detector. From an assessment of the counting rates for the products of reactions 1 and 2, we find that charge transfer comprises 80% of the product yield at 1.2 eV, increasing to ~96% at 3.4 eV.

Velocity map images for both products are determined as described in previous publications.<sup>16,17</sup> The present experiment is performed at unit mass resolution, and the duration of the ion signal along the flight axis associated with a single mass is only ~50 ns. This time is too short for effective slicing of the ion cloud for a particular mass.<sup>27</sup> We have employed the BASEX program<sup>28</sup> to carry out the inverse Abel transform required to extract correct product velocity and kinetic energy distributions from the images. Figure 1 shows raw velocity map images for charge-transfer ( $m/e = 15$ , left column) and proton-

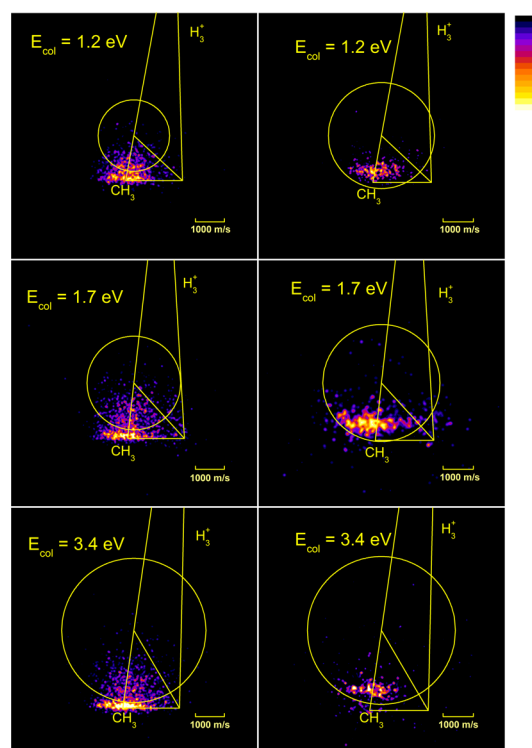


**Figure 1.** (Left column) Velocity map images for  $\text{CH}_3^+$  charge-transfer products at the three collision energies indicated. The kinematic Newton diagram appropriate for each energy is superimposed on the image. The circle at each collision energy describes the maximum charge-transfer product center of mass speed allowed by the sum of the collision energy and reaction endoergicity; the reactant vibrational energy is not included. (Right column) Velocity map images for  $\text{CH}_4^+$  proton-transfer products at the three collision energies indicated. Circles at each collision energy describe the maximum  $\text{CH}_4^+$  center of mass speed allowed by the sum of the collision energy and reaction exoergicity. The signal intensity scale is shown at the upper right.

transfer ( $m/e = 16$ , right column) products at collision energies of 1.2, 1.7, and 3.4 eV. The images represent Cartesian flux in center of mass coordinates, denoted  $P(u_x, u_y)$ .<sup>29</sup> Kinematic Newton diagrams appropriate for each of the collision energies are superimposed on the images.

The charge-transfer product images in Figure 1 show that the product velocities are equal to the corresponding incoming reactant velocities, indicative of long-range electron transfer that produces negligible momentum transfer. The fact that the product flux distributions lie outside of the circles defining the maximum product velocities allowed for vibrationally cold reactants demonstrates that reactant internal excitation is used to overcome the potential energy barrier of the reaction. Referring to Figure 1, each  $\text{H}_3^+$  reactant vibrational state would correspond to a Newton circle of different radius, increasing in size with increasing vibrational energy. The images show a sharp ridge of intensity that describes an arc intersecting the tip of the relative velocity vector. The Newton circle that describes the actual locus of product state velocities corresponds to approximately 0.66 eV of reactant vibrational energy, the charge-transfer reaction endoergicity. This ridge is elongated because of the broad speed distribution of the sonic flow from the pyrolysis source. This locus of points is consistent with  $\text{CH}_3^+$  products formed via resonant charge transfer, in which the initial speed of  $\text{CH}_3$  radicals and the final speed of  $\text{CH}_3^+$  ions are equal. The geometries of  $\text{CH}_3$  and  $\text{CH}_3^+$  are planar,<sup>30</sup>

and there is no significant change in molecular geometry upon ionization. Therefore, the Franck–Condon factor distribution is very narrow. In addition, each image shows a shadow of intensity that corresponds to the production of ions with center of mass speeds significantly smaller than those associated with resonant charge transfer.

These features are shown more clearly in the product kinetic energy distributions obtained by integrating the inverse Abel-transformed image data over angular coordinates according to eq 3

$$\langle P(E_T') \rangle_\theta = \int_0^\pi d\theta \sin \theta u P(u_x, u_y) \quad (3)$$

The center of mass speed and scattering angle are determined from a  $(u_x, u_y)$  pair as follows

$$|u| = \sqrt{u_x^2 + u_y^2} \quad (4)$$

$$\theta = \tan^{-1} \left( \frac{u_y}{u_x} \right) \quad (5)$$

In computing the kinetic energy distributions for the  $\text{CH}_3^+$  products, we are implicitly assuming that the  $(\text{H}, \text{H}_2)$  assembly resulting from neutralization of  $\text{H}_3^+$  moves as a unit, with small kinetic energy release. The sharpness of the  $\text{CH}_3^+$  distributions provides justification for this quasi-two-body product assumption and justifies use of the inverse Abel transform but does require us to consider the charge-transfer energy distributions as approximate. The quasi-two-body assumption is reminiscent of established treatments of collision-induced dissociation.<sup>31–33</sup> The left column of Figure 2 shows the kinetic energy distributions for the charge-transfer products. The distribution at the highest collision energy shows most clearly that it is comprised of two components; a sharp peak of width  $\sim 1$  eV is centered on the incident collision energy as expected for resonant charge transfer and a shoulder that extends to lower kinetic energy. The apparent structure in this part of the distributions, especially at 1.7 eV collision energy, is most likely within experimental error.

The images for the formation of  $\text{CH}_4^+$  by proton transfer are shown in the right column of Figure 1. They are very clearly displaced from the tip of the neutral beam velocity toward smaller center of mass speeds and indicate that  $\text{CH}_4^+$  products are formed in a direct “stripping” process in which the nascent products are formed in the direction of the incident  $\text{CH}_3$  reactant. However, the  $\text{CH}_4^+$  products are formed with center of mass speeds that are 15–25% larger than the predictions of the impulsive Spectator Stripping (SS) model,<sup>34</sup> in which the center of mass speed of the  $\text{H}_3^+$  reactant is the same as that of the  $\text{H}_2$  product. Thus, the center of mass speed of the  $\text{H}_2$  spectator remains constant. Significant vibrational motion in the approaching  $\text{H}_3^+$  reactants occurring on the time scale of chemical reaction suggests that there are strong interactions among the reactant atoms that invalidate the applicability of the simple SS model.

The kinetic energy distributions for the formation of  $\text{CH}_4^+$ , shown in the right panel of Figure 2, reveal that energy partitioning into the reaction products is described by sharp distributions of fwhm of approximately 1 eV at all collision energies. Although the energy partitioning is significantly different from the predictions of the impulsive SS model, the reaction does exhibit energy partitioning governed in large part by collision kinematics. When a light particle ( $\text{H}^+$ ) is

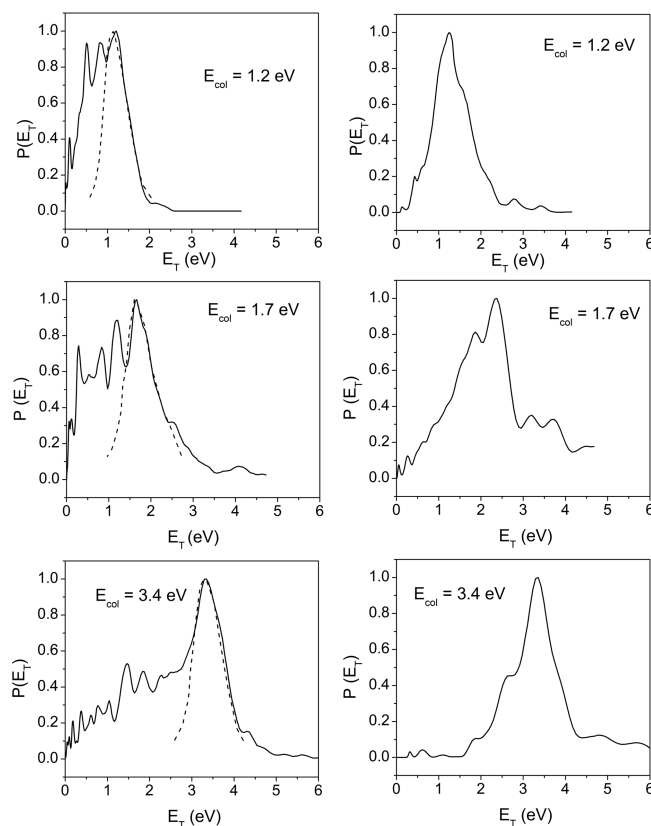


**Figure 2.** (Left column) Product kinetic energy distributions for  $\text{CH}_3^+$  charge-transfer products at three collision energies indicated. The distributions are computed from inverse Abel-transformed images using eqs 3–5. The dashed curves show schematically the kinetic energy distributions expected for energy-resonant charge transfer occurring in long-range collisions. The tail to lower energies arise from smaller impact parameter collisions in which incident translation is converted to product internal excitation. (Right column) Product kinetic energy distributions for  $\text{CH}_4^+$  proton-transfer products at three collision energies indicated. The apparent shoulder in the 1.7 eV distribution at energies above the peak is within the error limits of the data.

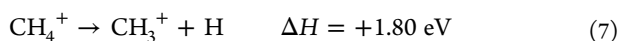
transferred from the  $\text{H}_2$  moiety to  $\text{CH}_3$ , the scaled and skewed potential energy profile that diagonalizes the quadratic form of the Hamiltonian<sup>35</sup> exhibits a skew angle  $\beta$  between the entrance and exit coordinates given by

$$\tan^2 \beta = \frac{m_{\text{H}} M_{\text{total}}}{m_{\text{CH}_3} m_{\text{H}_2}} \quad (6)$$

where  $M_{\text{total}}$  is the total mass of the collision system. For reaction 2, the skew angle  $\beta$  is  $38^\circ$ . This kinematic condition is very similar to the reaction motif Polanyi and co-workers have called “induced repulsive energy release”, in which incoming trajectories with enhanced translational energy access the “corner” of the potential energy surface where both the breaking bond and the forming bond are compressed.<sup>36</sup> This distorted molecular geometry propels the products through the exit channel with enhanced translation and little internal excitation. Although the mass combination in the present case differs from the classic heavy + light – heavy case discussed by Polanyi et al.,<sup>36</sup> the general features of induced repulsive energy release still appear to hold. Quantitative evidence for this reaction motif comes from the following considerations: as the collision energy increases from 1.2 to 1.7 eV, the most probable

product kinetic energy increases from 1.2 to about 1.9 eV. Within experimental error, all of the incremental reactant translational energy appears in the products. As the reactant translational energy increases from 1.7 to 3.4 eV, the most probable product translational energy increases from 1.9 to 3.2 eV. In this second, higher-energy case, the incremental translational energy of 1.7 eV produces a smaller increase in product translation, 1.3 eV, amounting to ~75% of the incremental product translation. Whether this decrease in the percentage of incremental reactant translation appearing in the product kinetic energy is significant is unclear and would require studies over a broader energy range to confirm. However, the data do confirm that the kinematics of proton transfer play an important role in directing reagent translation into product translational degrees of freedom.

At the collision energies of these experiments, a fraction of nascent  $\text{CH}_4^+$  products have sufficient energy to dissociate to  $\text{CH}_3^+$  via the reaction



If a fraction of the  $\text{CH}_3^+$  products that we observe could be attributed to reaction 7, those products would first appear in velocity space at threshold near the centroid of the collision system, where their barycentric speeds would be near zero. The  $\text{CH}_3^+$  products that we observe are not formed near the centroid but are displaced to larger velocities much more closely associated with charge transfer. Moreover, signal levels from unimolecular decay would be small fractions of the  $\text{CH}_4^+$  parent signals, which are already significantly smaller than those from charge transfer. The  $\text{CH}_3^+$  data therefore appear to be compatible with charge transfer but not with secondary decay of the products of proton transfer.

Although the internal energy distribution in the  $\text{H}_3^+$  ions is unknown in this experiment, a number of conclusions can be made. We can estimate the width of the distribution from experimental data. The total energy accessible to the products is the sum of the collision energy, the reactant vibrational energy, and the absolute value of the reaction exoergicity. Assuming that the largest observed kinetic energy release correlates with the total available energy, we can get a rough estimate of the internal excitation of  $\text{H}_3^+$ . For example, at a collision energy of 1.2 eV, reaction products appear to extend out to 2.0 eV. To form such products, the minimum vibrational energy of the system must be approximately  $2.0 \text{ eV} - (1.2 \text{ eV} - 0.66 \text{ eV})$ , or about 1.5 eV. The same method applied to the data at collision energies of 1.7 and 3.4 eV produces estimates of minimum excitation of 1.6 and 1.5 eV, respectively. These estimates are consistent with the calculations reported by Smith and Futrell.<sup>25</sup>

Most important, however, is the fact that endoergic charge transfer driven by reactant ions with vibrational energies in excess of the reaction barrier proceeds via energy resonance through large impact parameters. Irrespective of the reactant vibrational energy, the speeds of the  $\text{CH}_3$  nuclear framework, whether for the radical or the ion, are unchanged by electron transfer via this resonant process. This observation is supported by the work of Anderson and colleagues<sup>37</sup> in the  $\text{H}_2\text{CO}^+ + \text{C}_2\text{H}_2$  system, in which the authors comment that endoergic charge transfer appears to be controlled by Franck–Condon factors, “implying that it occurs at large inter-reactant separations, contrary to the expectation that endoergic reactions should require intimate collisions...” Although we do see evidence for such low impact parameter collisions, the

dominant process for charge transfer in the present case is precisely that noted by these authors.

In follow-up experiments, we plan to prepare  $\text{H}_3^+$  in a 10%  $\text{H}_2/90\%$  Ar mixture. This method takes advantage of the fact that the proton affinity of Ar is ~50  $\text{kJ mol}^{-1}$  smaller than that of  $\text{H}_2$ , resulting in removal of  $\text{H}_3^+$  reactants with more than 50  $\text{kJ mol}^{-1}$  of vibrational energy. This technique will significantly sharpen the internal energy distributions of  $\text{H}_3^+$  but will not yield energy-selected reactants.

This experiment is the first study of ion–radical reactions that provides direct measurements of product angular and kinetic energy distributions. Although well-established dynamical principles such as the role of Franck–Condon factors and collision kinematics provide a foundation for interpreting the data, these results will challenge theory to develop a more sophisticated understanding of the interactions that control reaction dynamics in radical systems. Ongoing studies in our lab are concerned with more complex radicals such as allyl and with ions having unpaired electrons. The latter reactions are examples of highly correlated systems, affording challenges to electronic structure theory and reaction dynamics. The present study suggests that there is much to be learned about both simple and complex ion–radical reactions, and close collaboration with theorists will advance the field.

## ■ EXPERIMENTAL METHOD

The crossed beam experimental arrangement is similar to that described in our previous publications.<sup>16,17</sup> Electrostatic shielding in the collision region has been enhanced with an improved electrode design that relies on apertures but adds cylindrical “curtains” similar to those described by Wester and co-workers.<sup>38</sup> The design shields the interaction region from poorly defined stray fields created by asymmetric grounded surfaces. A third aperture controlled by an additional independent pulse generator has been added to overcome the limited velocity mapping capabilities of the standard two-electrode configuration. The additional electrode improves corrections for chromatic aberration that arise from the finite thickness of the collision volume.

The free radical source, heated by 45 W of DC power, operates by pyrolyzing a 1% mixture of di-*tert*-butyl peroxide (DTBP) in He carrier gas at a total pressure of 3 atm. Experiments were carried out to ensure that all product ions are formed from  $\text{CH}_3$  radicals themselves and not by reactions with the precursor. The flow from the pyrolysis region is sonic under the operating conditions employed here.<sup>39</sup> Although we are unable to assess the internal excitation of the  $\text{CH}_3$  radicals from the source, a recent synchrotron radiation study of the threshold photoelectron spectroscopy of methyl radicals produced from a continuous pyrolytic source with similar heating power indicated rotational and vibrational temperatures of 400 and 500–600 K, respectively.<sup>40</sup> The internal energy contribution to the system from the radical beam is thus considered to be small, on the order of 0.05 eV.

The ion beam is produced by electron impact on hydrogen gas at high pressure in the electron impact source, which we have described previously, and contains significant vibrational excitation, as discussed above.<sup>41</sup>

Because the focusing conditions for VMI are very different from those that optimize mass resolution, we have performed careful experiments to assess crosstalk between adjacent mass peaks. A calibration experiment employing the  $\text{N}_2^+ + \text{N}_2$  resonant charge-transfer reaction showed that the  $m/e = 28$

charge-transfer signal produces crosstalk at  $m/e = 29$ , that is, at longer delay time, in precisely the same region of velocity space, at a signal level of less than 1% of the  $m/e = 28$  signal. We also carried out an experiment on the endoergic charge-transfer system  $\text{CO}^+ + \text{CH}_3$ , in which we observed a strong  $\text{CH}_3^+$  signal at  $m/e = 15$ . Crosstalk at  $m/e = 16$  was at background level. These experiments provide clear evidence that crosstalk from the intense  $\text{CH}_3^+$  signal from reaction 1 is not responsible for any of the  $m/e = 16$  signal.

## AUTHOR INFORMATION

### Corresponding Author

\*E-mail: jfarrar@UR.rochester.edu.

### Notes

The authors declare no competing financial interest.

## ACKNOWLEDGMENTS

The authors acknowledge support for this work under National Science Foundation Grants CHE-1012303 and CHE-1265406. We thank Professor Domenico Stranges for his assistance with the design of the pyrolysis source and Professor Piero Casavecchia for providing SiC pyrolysis tubes. We are also grateful to Professors Cheuk-Yiu Ng and Scott Anderson for helpful conversations. E.C. expresses appreciation for financial support provided by the Austrian Academy of Sciences.

## REFERENCES

- (1) Thomson, J. J. On the Nature of X3, the Substance Giving The '3' Line. In *Rays of Positive Electricity*; Longman, Green, and Company: Essex, U.K., 1913; pp 116–122.
- (2) Gioumousis, G.; Stevenson, D. P. Reactions of Gaseous Molecule Ions with Gaseous Molecules. 5. Theory. *J. Chem. Phys.* **1958**, *29*, 294–299.
- (3) Zhang, X.; Bierbaum, V. M.; Ellison, G. B.; Kato, S. Gas-Phase Reactions of Organic Radicals and Diradicals with Ions. *J. Chem. Phys.* **2004**, *120*, 3531–3534.
- (4) Zhang, X.; Kato, S.; Bierbaum, V. M.; Nimlos, M. R.; Ellison, G. B. Use of a Flowing Afterglow SIFT Apparatus to Study the Reactions of Ions with Organic Radicals. *J. Phys. Chem. A* **2004**, *108*, 9733–9741.
- (5) Russell, A. L.; Rohrs, H. W.; Read, D.; Giblin, D. E.; Gaspar, P. P.; Gross, M. L. Radical Cation/Radical Reactions: A Fourier Transform Ion Cyclotron Resonance Study of Allyl Radical Reacting with Aromatic Radical Cations. *Int. J. Mass Spectrom.* **2009**, *287*, 8–15.
- (6) Sawyer, J. C.; Shuman, N. S.; Wiens, J. P.; Viggiano, A. A. Kinetics and Product Branching Fractions of Reactions Between a Cation and a Radical:  $\text{Ar}^+ + \text{CH}_3$  and  $\text{O}_2^+ + \text{CH}_3$ . *J. Phys. Chem. A* **2015**, *119*, 952–958.
- (7) Kohn, D. W.; Clauberg, H.; Chen, P. Flash Pyrolysis Nozzle for Generation of Radicals in a Supersonic Jet Expansion. *Rev. Sci. Instrum.* **1992**, *63*, 4003–4005.
- (8) Blush, J. A.; Clauberg, H.; Kohn, D. W.; Minsek, D. W.; Xu, Z.; Chen, P. Photoionization Mass and Photoelectron-Spectroscopy of Radicals, Carbenes and Biradicals. *Acc. Chem. Res.* **1992**, *25*, 385–392.
- (9) Chandler, D. W.; Houston, P. L. Two-Dimensional Imaging of State-Selected Photodissociation Products Detected by Multiphoton Ionization. *J. Chem. Phys.* **1987**, *87*, 1445–1447.
- (10) Eppink, A.; Parker, D. H. Velocity Map Imaging of Ions and Electrons Using Electrostatic Lenses: Application in Photoelectron and Photofragment Ion Imaging of Molecular Oxygen. *Rev. Sci. Instrum.* **1997**, *68*, 3477–3484.
- (11) Houston, P. L. Snapshots of Chemistry — Product Imaging of Molecular Reactions. *Acc. Chem. Res.* **1995**, *28*, 453–460.
- (12) Mikosch, J.; Fruhling, U.; Trippel, S.; Schwalm, D.; Weidemuller, M.; Wester, R. Velocity Map Imaging of Ion–Molecule Reactive Scattering: The  $\text{Ar}^+ + \text{N}_2$  Charge Transfer Reaction. *Phys. Chem. Chem. Phys.* **2006**, *8*, 2990–2999.
- (13) Mikosch, J.; Trippel, S.; Eichhorn, C.; Otto, R.; Lourderaj, U.; Zhang, J. X.; Hase, W. L.; Weidemuller, M.; Wester, R. Imaging Nucleophilic Substitution Dynamics. *Science* **2008**, *319*, 183–186.
- (14) Zhang, J. X.; Mikosch, J.; Trippel, S.; Otto, R.; Weidemuller, M.; Wester, R.; Hase, W. L.  $\text{F}^- + \text{CH}_3\text{I} \rightarrow \text{FCH}_3 + \text{I}^-$  Reaction Dynamics. Nontraditional Atomistic Mechanisms and Formation of a Hydrogen-Bonded Complex. *J. Phys. Chem. Lett.* **2010**, *1*, 2747–2752.
- (15) Wester, R. Velocity Map Imaging of Ion–Molecule Reactions. *Phys. Chem. Chem. Phys.* **2014**, *16*, 396–405.
- (16) Pei, L.; Farrar, J. M. Imaging Ion–Molecule Reactions: Charge Transfer and C–N Bond Formation in the  $\text{C}^+ + \text{NH}_3$  System. *J. Chem. Phys.* **2012**, *136*, 204305.
- (17) Pei, L.; Farrar, J. M. Ion Imaging Study of Reaction Dynamics in the  $\text{N}^+ + \text{CH}_4$  System. *J. Chem. Phys.* **2012**, *137*, 154312.
- (18) Thermodynamic parameters taken from NIST Chemistry WebBook; Mallard, W. G., Linstrom, P. J., Eds.; NIST Standard Database Number 69; National Institute of Standards and Technology: Gaithersburg, MD, 2000; <http://webbook.nist.gov/chemistry/>.
- (19) Oka, T. Interstellar  $\text{H}_3^+$ . *Proc. Natl. Acad. Sci. U.S.A.* **2006**, *103*, 12235–12242.
- (20) Drossart, P.; Maillard, J. P.; Caldwell, J.; Kim, S. J.; Watson, J. K. G.; Majewski, W. A.; Tennyson, J.; Miller, S.; Atreya, S. K.; Clarke, J. T.; et al. Detection of  $\text{H}_3^+$  on Jupiter. *Nature* **1989**, *340*, 539–541.
- (21) Trafton, L. M.; Geballe, T. R.; Miller, S.; Tennyson, J.; Ballester, G. E. Detection of  $\text{H}_3^+$  from Uranus. *Astrophys. J.* **1993**, *405*, 761–766.
- (22) Geballe, T. R.; Oka, T. Detection of  $\text{H}_3^+$  in Interstellar Space. *Nature* **1996**, *384*, 334–335.
- (23) van Dishoeck, E. F. ISO Spectroscopy of Gas and Dust: From Molecular Clouds to Protoplanetary Disks. *Annu. Rev. Astron. Astrophys.* **2004**, *42*, 119–167.
- (24) Bowers, M. T.; Elleman, D. D. Analysis of Ion–Molecule Reactions in Hydrogen–Methane Mixtures Using Ion-Cyclotron Resonance. *J. Am. Chem. Soc.* **1970**, *92*, 1847–1854.
- (25) Smith, D. L.; Futrell, J. H. Internal Energy Effects on the Reaction of  $\text{D}_3^+$  with  $\text{CH}_4$ . *J. Phys. B: At. Mol. Opt. Phys.* **1975**, *8*, 803–815.
- (26) Pei, L.; Yang, N. Private communication.
- (27) Townsend, D.; Miniti, M. P.; Suits, A. G. Direct Current Slice Imaging. *Rev. Sci. Instrum.* **2003**, *74*, 2530–2539.
- (28) Dribinski, V.; Ossadtchi, A.; Mandelshtam, V. A.; Reisler, H. Reconstruction of Abel-Transformable Images: The Gaussian Basis-Set Expansion Abel Transform Method. *Rev. Sci. Instrum.* **2002**, *73*, 2634–2642.
- (29) Friedrich, B.; Herman, Z. Processing of Ion–Molecule Beam Scattering Data: Framework of Scattering Diagrams and Derived Quantities. *Collect. Czech. Chem. Commun.* **1984**, *49*, 570–585.
- (30) Chau, F. T. Molecular Parameters of Excited Molecules and Ions. Part V. The Methyl Radical and its Ions. *J. Mol. Struct.: THEOCHEM* **1985**, *119*, 281–294.
- (31) Herman, Z.; Futrell, J. H.; Friedrich, B. A Beam Scattering Study of the Collision-Induced Dissociation of Polyatomic Ions  $\text{CH}_4^+$  and  $\text{C}_3\text{H}_8^+$  at eV Collision Energies. *Int. J. Mass Spectrom. Ion Processes* **1984**, *58*, 181–199.
- (32) Shukla, A. K.; Qian, K. G.; Howard, S. L.; Anderson, S. G.; Sohlberg, K. W.; Futrell, J. H. Collision-Induced Dissociation Reaction Dynamics of the Acetone Molecular Ion. *Int. J. Mass Spectrom. Ion Processes* **1989**, *92*, 147–169.
- (33) Shukla, A. K.; Qian, K.; Anderson, S.; Futrell, J. H. Fundamentals of Tandem Mass-Spectrometry — A Dynamics Study of Simple C–C Bond-Cleavage in Collision-Activated Dissociation of Polyatomic Ions At Low-Energy. *J. Am. Soc. Mass Spectrom.* **1990**, *1*, 6–15.
- (34) Henglein, A.; Lacmann, K.; Jacobs, G. Collision Mechanism in Bimolecular Reactions. I. Theory and Experimental Determination Methods of the Velocity Spectrum of the Products Resulting from the Simple H-Transfer Reactions of  $\text{X}^+ + \text{H}_2 \rightarrow \text{XH}^+ + \text{H}$  Type. *Ber. Bunsen-Ges. Phys. Chem.* **1965**, *69*, 279.

(35) Hirschfelder, J. O. Coordinates Which Diagonalize the Kinetic Energy of Relative Motion. *Int. J. Quantum Chem. Symp.* **1969**, *3*, 17–31.

(36) Ding, A. M. G.; Kirsch, L. J.; Perry, D. S.; Polanyi, J. C.; Schreiber, J. L. Effect of Changing Reagent Energy on Reaction Probability and Product Energy-Distribution. *Faraday Discuss. Chem. Soc.* **1973**, *55*, 252–276.

(37) Liu, J. B.; Van Devener, B.; Anderson, S. L. Vibrational Mode and Collision Energy Effects on Reaction of  $\text{H}_2\text{CO}^+$  with  $\text{C}_2\text{H}_2$ : Charge State Competition and the Role of Franck–Condon Factors in Endoergic Charge Transfer. *J. Chem. Phys.* **2005**, *123*, 204313.

(38) Stei, M.; von Vangerow, J.; Otto, R.; Kelkar, A. H.; Carrascosa, E.; Best, T.; Wester, R. High Resolution Spatial Map Imaging of a Gaseous Target. *J. Chem. Phys.* **2013**, *138*, 214201.

(39) Guan, Q.; Urness, K. N.; Ormond, T. K.; David, D. E.; Ellison, G. B.; Daily, J. W. The Properties of a Micro-Reactor for the Study of the Unimolecular Decomposition of Large Molecules. *Int. Rev. Phys. Chem.* **2014**, *33*, 447–487.

(40) Cunha de Miranda, B. K.; Alcaraz, C.; Elhanine, M.; Noller, B.; Hemberger, P.; Fischer, I.; Garcia, G. A.; Soldi-Lose, H.; Gans, B.; Vieira Mendes, L. A.; et al. Threshold Photoelectron Spectroscopy of the Methyl Radical Isotopomers,  $\text{CH}_3$ ,  $\text{CH}_2\text{D}$ ,  $\text{CHD}_2$  and  $\text{CD}_3$ : Synergy between VUV Synchrotron Radiation Experiments and Explicitly Correlated Coupled Cluster Calculations. *J. Phys. Chem. A* **2010**, *114*, 4818–4830.

(41) Udseth, H.; Giese, C. F.; Gentry, W. R. Transition Probabilities and Differential Cross-Sections for Vibrational Excitation in Collisions of  $\text{H}^+$  with  $\text{H}_2$ , HD, and  $\text{D}_2$ . *Phys. Rev. A* **1973**, *8*, 2483–2493.